Mechanical deformation of WC-Co composite micropillars under uniaxial compression

J.M. Tarragó[1,2], J.J. Roa[1,2], E. Jiménez-Piqué[1,2], E. Keown[3], J. Fair[3] and L. Llanes[1,2;*]

[1]*CIEFMA, Departament de Ciència dels Materials i Enginyeria Metal·lúrgica, Universitat Politècnica de Catalunya, Barcelona, 08028, Spain*

[2]*CRnE, Centre de Recerca en Nanoenginyeria, Universitat Politècnica de Catalunya, Barcelona, 08028, Spain*

[3]*Sandvik Hyperion, Coventry, CV4 0XG, UK*

ABSTRACT

In this work, WC-Co micropillars machined by focused ion beam have been tested under uniaxial compression to investigate the stress-strain behavior and associated deformation mechanisms. The results indicate that yielding phenomena is evidenced by multiple strain bursts. Experimental data is found to fall within the bounds defined by the mechanical responses expected for an unconstrained Co-binder like model alloy and a bulk-like constrained binder region in WC-Co composites; capturing then local phase assemblage and crystal orientation effects.

Keywords: Cemented carbides, Microcompression testing, Plastic deformation, Damage mechanisms, Focused Ion Beam (FIB).

*Author to whom correspondence should be addressed. Electronic mail: luis.miguel.llanes@upc.edu

INTRODUCTION

Understanding the deformation of ductile metallic ligaments constrained by a hard ceramic phase is a key feature for determining effective toughening in metal reinforced ceramic-base composites [1–3]. WC-Co cemented carbides, also referred to as hardmetals, are one of the most extensively employed “tailor-made” composites and a clear example of this type of material. It consist of two interpenetrating-phase networks (i.e. soft/ductile metallic binder and hard/brittle ceramic particles), where toughening through constrained deformation of the ductile phase is highly effective. As a consequence, they exhibit outstanding toughness level as related to the energy required to plastically deform the metallic bridging ligaments that develop behind the tip of preexisting or service-induced cracks [4–9]. During the last decades, extensive effort has been devoted to predict the mechanical response of the constrained ductile bridges and its contribution to the fracture toughness of the composite. As a result, several models have been presented [1,2,5,7,10]. However, these models are based on the macromechanical response of the composites investigated, and more important, are limited due to the scarce information on the interactive deformation of the constitutive phases at the microstructural length scale.

High toughness levels of cemented carbides have also been invoked as the result of the effective interaction between intrinsic residual stress state and external applied stress [11-15]. In this regard, it is known that very large thermal residual stresses (TRS) develop in these materials as they are cooled from sintering temperature, due to the large difference between the thermal expansion coefficients of both constituent phases.

The thermal expansion coefficient of Co is more than twice that of WC, and therefore high tensile TRS can be expected in the metallic phase, while the overall stress state of the WC particles is compressive [11]. However, wide stress ranges have been evidenced in the local stress states of both phases, including tensile stresses at some WC angularities [11]. Under the application of external loads, TRS interact with the applied stress field and strongly influence the plastic deformation of the system. During uniaxial compressive loading, main plastic deformation is accommodated by the binder phase; although small plastic strains have been also evidenced in WC particles [12]. In the axial direction, mean TRS in the binder phase opposes the compressive applied stress, but in the transverse direction the tensile stress state that results from the Poisson effect adds to the TRS stresses resulting in binder flow in this direction [12,14]. Nevertheless, addressing the exact stress-state produced under the application of compression loads is extremely complicated because the macroscopic plasticity is the result of the aggregation of multiple micro-scale yield events within particular phases. Furthermore, during loading the strain and stress state of the system is in constant evolution due to the continuous redistribution and cancellation of internal plastic strains between phases [12].

Recent advances in micro- and nano- fabrication and testing systems have enabled the assessment of deformation behavior of bulk materials on a microscopic scale. The use of focused ion beam (FIB) technique combined with nanoindentation has provided the means for machining and uniaxial compression testing of micropillar samples [16]. Within this context, while significant effort has been dedicated to study the mechanical

behavior of single-crystals or boundary-containing metallic systems [17], less attention has been paid to the case of composite materials (e.g. Refs. [18,19]), and particularly those combining soft and hard phases (e.g. Refs. [20,21]). To the best knowledge of the authors, experimental micromechanics studies on WC-Co composites reduce to two recent reports [22,23]. In one of them, micropillar compression testing of hardmetals was conducted by Csanádi *et al.*, but their investigation was limited to evaluation of the deformation characteristics of the hard carbide phase [22]. On the other hand, Trueba and coworkers documented and analyzed fracture events in WC-Co cemented carbides by microbeam testing and finite element modeling [23]. It is the aim of this study to bring insights on the mechanical deformation and failure behavior of ceramic-metal composite materials through the compression of micropillars consisting of Co-binder ligaments constrained by their surrounding WC carbides. In doing so, special attention is paid to document and analyze microstructural effects regarding yield strength and constraining degree.

EXPERIMENTAL PROCEDURE

The micropillars were carved into the surface of a coarse-grained WC-15%$_{wt.}$Co composite by means of a Zeiss Neon 40 FIB milling system operated at 5 kV. Milling process was carried out in two stages in order to minimize damage by impinging ions. Initially, a ring with outer and inner diameters of 15 μm and 4 μm was carved using an ion beam current of 4 nA. Afterwards, micropillars with final diameters varying from 2.5 to 3 μm, aspect ratios ranging from 2 to 2.5 and taper angles between 2º and 3º, were

shaped using a 500 pA current. Two examples of micropillars before compression tests are shown in insets within **Figure 1**. The micropillars were uniaxially compressed using a Nanoindenter XP (MTS) fitted with a 5 μm diameter flat diamond-punch at a constant displacement rate of 10 nm/s (initial strain rates around 0.0015 s^{-1}). Load-displacement data was continuously recorded in the same way as being practiced in nanoindentation measurements. Nominal stresses and strains were directly determined from the load-displacements curves, using the diameter at one quarter of the way down the pillar (as most deformation occurred in this region) and its effective gauge length, respectively. Four micropillars were indented at different depths corresponding to maximum axial strains (ε_f) of 2.9, 3.8, 4.4 and 5.5%. Irreversible deformation and failure mechanisms have been directly examined by means of Field Emission Scanning Electron Microscopy (FESEM), as well as by serial sectioning and imaging using the FIB/FESEM system.

RESULTS AND DISCUSSION

FESEM micrographs of two micropillars compressed up to maximum strains of 2.9 and 4.4% are shown in **Figure 1**, before (insets) and after compression tests. Two different shearing mechanisms are identified in the FESEM micrographs. The first one (very clear in **Figure 1b**) takes place at the interface between the WC particle and the metallic binder, at angles comprised between 30º and 45º with respect to the compression axis. Detailed analysis permits to discern that shearing does not occur exactly at the interface, but rather proceeds within the binder very close to the phase boundary and parallel to it. This finding is consistent with the fact that binder regions adjacent to carbide/binder

interfaces are preferred crack growth locations, due to coincidence of high plastic strains and maximum triaxiality conditions [6]. The second deformation mechanism develops at the grain boundaries between contiguous WC crystals. Although it may be speculated that observation of different shearing/cracking mechanisms should be dependent upon specific crystal orientation and local phase arrangement (i.e. effective constraining degree) within the pillar, it is clear that interfaces, between either binder and carbide or carbides themselves, are favorable points for driving irreversible deformation and failure events under macroscopic compressive stresses.

To better understand the deformation/failure mechanisms under uniaxial compression tests, the micropillar compressed up to a strain of 4.4% was sequentially cross sectioned and visualized using the FIB/FESEM system. Thus, micrographs corresponding to the interior of the deformed pillar are shown in **Figure 2** where the most prominent events are marked with white arrows. In all three micrographs a glide system within the binder adjacent to the interface with the WC particles can be appreciated (at an angle of about 42º with respect the compression axis). Furthermore, in the central image (**Figure 2b**), a microcrack running parallel to the carbide/binder interface (but still within the binder phase) is also identified. This microcrack probably stems from the propagation of the carbide-carbide interface microcrack that is at the same position in **Figure 2a**. Binder regions close to carbide corners combine large concentrations of strains and/or stress triaxiality; thus, they are favorable zones for early flow and/or crack propagation [6]. On the other hand, all carbide-carbide interfaces are affected by compression loading, pointing out that they are weak links in these ceramic-metal composites [5]. Evidence of

extensive plastic deformation within the binder is observed in **Figure 2c**. It may come from less effective constraining or plastic flow associated with local interaction between TRS and applied stress. In this regard, it should be pointed out that the already complex point-to-point residual stress state in both phases may be relaxed or enhanced by local tensile stresses related to the Poisson effect under the nominally compressive applied one [12,14]. Such deformation may take place through mechanical twinning, planar slip and/or phase transformation (fcc to hcp) [24–27]. Identification of the specific irreversible deformation mechanisms would require an additional transmission electron microscopy analysis, and it is beyond the scope of this study. Finally, the activation of a slip system is detected within the carbide placed on the top of the pillar (**Figures 2a** and **2b**). Similar features have been observed by compressing micropillars carved in WC prismatic planes [22] and are associated with a splitting dislocation reaction in the $\{10\bar{1}0\}\langle 11\bar{2}3\rangle$ predominant slip system [28,29].

The loading-unloading mechanical response, resulting from monotonic compression at different strains of hardmetal micropillars, is shown as stress-strain curves in **Figure 3**. Elastic modulus expected for metallic binder or tungsten carbide phases, on the basis of its measured bulk stiffness, are also included for comparison purposes in the top right corner of the figure. As expected, elastic modulus data resulting from the unloading stress-strain curves of the WC-Co compressed micropillars are within values of this parameter for the individual phases. On the other hand, strain-hardening response (loading curve) is variable, indicating its dependence on crystal orientation and local phase arrangement. Here it should be noticed that binder phase within hardmetals

usually form regions of a single-crystallographic orientation up to 50 times greater than the mean size of the WC grains [30]. In this regard, different micropillars indeed consist of a binder phase with a well-defined (and unique) crystal orientation, cementing several carbides with distinct crystal orientations. Furthermore, it must be considered that TRS may be either relieved by the used milling procedure or relaxed depending on the effective microstructure length scale / micropillar diameter [11–15]. Indeed, a deeper investigation of mechanical response of micropillars with larger diameters or hardmetal grades with finer microstructures seems to be key for validating real constraining effects within these small-scale specimens, as compared to the ones existing in macroscopic samples. These referred issues are not addressed in this work, but they are highlighted as interesting topics for future research. As a final consequence, each tested micropillar should be preliminary described as a unique system, whose initial residual stress state and constraining scenario is strongly linked to its particular microstructural assemblage.

Compression curves show a linear stress-strain relationship prior to reaching the yield point for each micropillar tested. Yielding phenomena is evidenced by early (pop-in) strain bursts. As the material strain hardens, additional strain bursts are evidenced. First and subsequent strain bursts take place at different stress levels for each micropillar. The fact that all micropillars tested exhibited curves with discontinuities would suggest that they are physically related to activation of shearing/cracking events within a scenario of limited (and heterogeneous) plasticity, and rather independent of the binder crystal orientation. Accordingly, all of them may be considered as discrete microscopic

yielding events. However, gathering of specific information that could validate this hypothesis requires in-situ observation of micropillars as they are loaded. Also, information on the point to point thermal residual stresses state may be helpful to depict strain-burst events evidenced in the curves. Finally, clear evidence of irreversible deformation is observed in stress-strain curves after unloading.

Pop-in (strain burst) events detected in the stress-strain compression curves are plotted in **Figure 4**. Stress levels associated with these events follow a linear trend with applied strain. Early pop-ins are detected at stress levels between 0.6 and 1.7 GPa, whereas those evidenced at higher strains occurred at stress levels ranging from 1.0 to 3.1 GPa. These strain bursts may be related to the different irreversible deformation and failure events evidenced in the cross-sections views of the compressed pillars, as shown in **Figure 2**. Considering the softer character of the metallic binder, it would be expected that a large proportion of pop-ins registered are associated with deformation events taking place in the binder. Within this context, data gathered in **Figure 4** would effectively reflect the "yield stress" range for the constrained ductile ligaments, variable depending on orientation and constraining, the latter including free-surface and TRS-applied stress interaction issues. However, it should be recalled that plastic deformation phenomena was also evidenced within carbides (**Figures 2a** and **2b**), even though applied stresses were much lower than intrinsic yield stress values reported for WC phase (i.e. ~ 6-7 GPa) [22]. As referred above, it would sustain the synergic interaction of deformation phenomena taking place within the constitutive phases, particularly in regions close to interfaces and neighboring geometry irregularities of particles, as well

as the wide range of TRS for WC (compressive in average but tensile in specific regions) due to the particle shape and the microstructure [14].

Following the above ideas, data plotted in **Figure 4** would depict the intrinsic flow stress range for the metallic binder, depending on orientation and local constraining effects. Hence, limit values for such flow stress range should correspond to those exhibited by (1) completely unconstrained binder in the lower side and (2) highly constrained metallic phase in the upper one. Data for the former may be attained from the systematic and unique study on the mechanical properties of dilute Co-W-C alloys (i.e. model binder-like alloys corresponding to cobalt-rich solid solutions strengthened by dissolved tungsten and carbon) carried out by Roebuck and Almond [25]. These researchers report yield stress values for bulk Co-W-C alloys ranging from 0.4 to 0.8 GPa, depending on W and C additions. The fact that such a range is in excellent agreement with the lower bound data plotted in **Figure 4** (earliest pop-ins registered in the micropillar compression tests), points out the effective unconstrained nature of some binder regions in the tested specimens, i.e. true microstructural size effects. Regarding data for yielding of highly constrained binder, Sigl and coworkers [5,6] estimated values in the range from 2.2 to 3.7 GPa for a set of hardmetals with different binder content and carbide grain size. These values were deduced by implementing a Hall-Petch type relation for the onset of plastic flow in the soft phase of two-phase materials, as proposed by Chou [31]. Such a range is also in satisfactory agreement with the upper bound data included in **Figure 4**, and will correspond to binder yielding under highly constraining conditions. In general, most of the experimental data gathered fill the

intermediate gap between the referred bands; thus, capturing local phase arrangement (constraining degree) and crystal orientation effects. It will indicate micropillar compression testing as a suitable method for evaluating local mechanical response in WC-Co composites with the purpose of tailoring new and improved microstructural combinations, regarding both chemical nature as well as phase assemblage. This may be critical nowadays as the market of tool and wear-resistant component demands for new material configurations with enhanced properties composed of non-critical accessible materials.

SUMMARY

WC-Co composite micropillars (about 3 μm in diameter) consisting of few Co binder regions surrounded by hard particles have been FIB-milled and tested under uniaxial compression. Results reveal that boundaries between either carbide and binder or carbide crystals are preferential sites for irreversible deformation and failure phenomena. Plasticity is mostly evidenced within the softer metallic binder. However, even in this case, deformation takes place in regions adjacent to carbide-binder interface where maximum triaxiality stress conditions prevail. Stress-strain curves reveal several strain bursts at different stress levels, ranging from 0.6 to 3.1 GPa. They follow a linear trend as a function of imposed strain. These stress levels are comprised between the flow stresses values expected for an unconstrained Co-binder like model alloy and a highly constrained binder region in bulk WC-Co composites. Such variable flow stress is rationalized on the basis of different crystal orientation and local phase assemblage, the latter directly related to constraining degree (including free surface and TRS-applied

stress interaction effects) within the tested micropillars. This investigation provides a new insight into the microstructural design of ductile metal reinforced ceramic-base composites, on the basis of micropillar compression tests as a valid and effective experimental procedure for evaluation of mechanical response of these materials at the microscopic level.

ACKNOWLEDGEMENTS

The authors thank Trifon Trifonov at the CRnE for helping with the FIB-milling of the microcompression specimens. This work was financially supported by the Spanish Ministerio de Economía y Competitividad (Grant MAT2012-34602). Additionally, J.M. Tarragó and J.J. Roa would like to acknowledge financial support received from the collaborative Industry-University program between Sandvik Hyperion and Universitat Politècnica de Catalunya (PhD scholarship) and the Juan de la Cierva Programme (Grant number: JCI-2012–14454), respectively.

REFERENCES

[1] Evans AG, McMeeking RM. On the toughening of ceramics by strong reinforcements. Acta Metall 1986;34:2435–41.

[2] Ashby MF, Blunt FJ, Bannister M. Flow characteristics of highly constrained metal wires. Acta Metall 1989;37:1847–57.

[3] Riesch J, Buffiere J-Y, Höschen T, di Michiel M, Scheel M, Linsmeier C, You J-H. In situ synchrotron tomography estimation of toughening effect by semi-ductile fibre reinforcement in a tungsten-fibre-reinforced tungsten composite system. Acta Mater 2013;61:7060–71.

[4] Krstic VD. On the fracture of brittle-matrix/ductile-particle composites. Philos Mag A 1983;48:695–708.

[5] Sigl LS, Fischmeister HF. On the fracture toughness of cemented carbides. Acta Metall Mater 1988;36:887–97.

[6] Fischmeister HF, Schmauder S, Sigl LS. Finite element modelling of crack propagation in WC- Co hard metals. Mater Sci Eng A 1988;105/106:305–11.

[7] Pezzotti G, Huebner H, Suenobu H, Orfeo S, Nishida T. Analysis of near-tip crack bridging in WC/Co cermet. J Eur Ceram Soc 1999;19:119–23.

[8] McVeigh C, Liu WK. Multiresolution modeling of ductile reinforced brittle composites. J Mech Phys Solids 2009;57:244–67.

[9] Tarragó JM, Jimenez-Piqué E, Turón-Viñas M, Rivero L, Al-Dawery I, Schneider L, Llanes L. Fracture and fatigue behavior of cemented carbides: 3D focused ion beam tomography of crack-microstructure interactions. Int J Powder Metall 2014;50:1–10.

[10] Armstrong RW, Cazacu O. Indentation fracture mechanics toughness dependence on grain size and crack size: Application to alumina and WC–Co. Int J Refract Met Hard Mater 2006;24:129–34.

[11] Livescu V, Clausen B, Paggett JW, Krawitz AD, Drake EF, Bourke MAM. Measurement and modeling of room temperature co-deformation in WC–10wt.% Co. Mater Sci Eng A 2005;399:134–40.

[12] Paggett JW, Krawitz AD, Drake EF, Bourke MAM, Livescu V, Claussen B, Brown DW. In situ loading response of WC–Ni: Origins of toughness. Int J Refract Met Hard Mater 2006;24:122–8.

[13] Krawitz AD, Venter AM, Drake EF, Luyckx SB, Clausen B. Phase response of WC–Ni to cyclic compressive loading and its relation to toughness. Int J Refract Met Hard Mater 2009;27:313–6.

[14] Krawitz a. D, Drake EF, Clausen B. The role of residual stress in the tension and compression response of WC–Ni. Mater Sci Eng A 2010;527:3595–601.

[15] Krawitz A, Drake E. Residual stresses in cemented carbides — An overview. Int J Refract Met Hard Mater 2015;49:27–35.

[16] Uchic MD, Dimiduk DM, Florando JN, Nix WD. Sample dimensions influence strength and crystal plasticity. Science 2004;305:986–9.

[17] Greer JR, De Hosson JTM. Plasticity in small-sized metallic systems: Intrinsic versus extrinsic size effect. Prog Mater Sci 2011;56:654–724.

[18] Guo Q, Greer JR. Compressive properties of interface-containing Cu–Fe nano-pillars. Scr Mater 2011;66:272–5.

[19] Li N, Mara NA, Wang J, Dickerson P, Huang JY, Misra A. Ex situ and in situ measurements of the shear strength of interfaces in metallic multilayers. Scr Mater 2012;67:479–82.

[20] Singh DRP, Chawla N, Tang G, Shen Y-L. Micropillar compression of Al/SiC nanolaminates. Acta Mater 2010;58:6628–36.

[21] Shih C, Katoh Y, Leonard KJ, Bei H, Lara-Curzio E. Determination of interfacial mechanical properties of ceramic composites by the compression of micro-pillar test specimens. J Mater Sci 2013;48:5219–24.

[22] Csanádi T, Bl'anda M, Duszová A, Chinh NQ, Szommer P, Duska J. Deformation characteristics of WC micropillars. J Eur Ceram Soc 2014;34:4099–103.

[23] Trueba M, Aramburu A, Rodríguez N, Iparraguirre I, Elizalde MR, Ocaña I, Sánchez JM, Martínez-Esnaola JM. "In-situ" mechanical characterisation of WC–Co hardmetals using microbeam testing. Int J Refract Met Hard Mater 2014;43:236–40.

[24] Sarin VK, Johannesson T. On the deformation of WC-Co cemented carbides. Met Sci 1975;9:472–6.

[25] Roebuck B, Almond EA. The influence of composition, phase transformation and varying the relative F.C.C. and H.C.P. phase contents on the properties of dilute Co-W-C Alloys. Mater Sci Eng 1984;66:179–94.

[26] Vasel CH, Krawitz AD, Drake EF, Kenik EA. Binder deformation in WC-(Co, Ni) cemented carbide composites. Metall Mater Trans A 1985;16A:2309–17.

[27] Erling G, Kursawe S, Luyck S, Sockel HG. Stable and unstable fracture surface features in WC-Co. J Mater Sci Lett 2000;19:437–8.

[28] Hibbs MK, Sinclair R. Room-temperature deformation mechanisms and the defect structure of tungsten carbide. Acta Metall 1981;29:1645–54.

[29] Lay S. HRTEM investigation of dislocation interactions in WC. Int J Refract Met Hard Mater 2013;41:416–21.

[30] Mingard KP, Roebuck B, Marshall J, Sweetman G. Some aspects of the structure of cobalt and nickel binder phases in hardmetals. Acta Mater 2011;59:2277–90.

[31] Chou YT. Equilibrium of linear dislocation arrays in heterogeneous materials. J Appl Phys 1966;37:2425–9.

LIST OF FIGURES

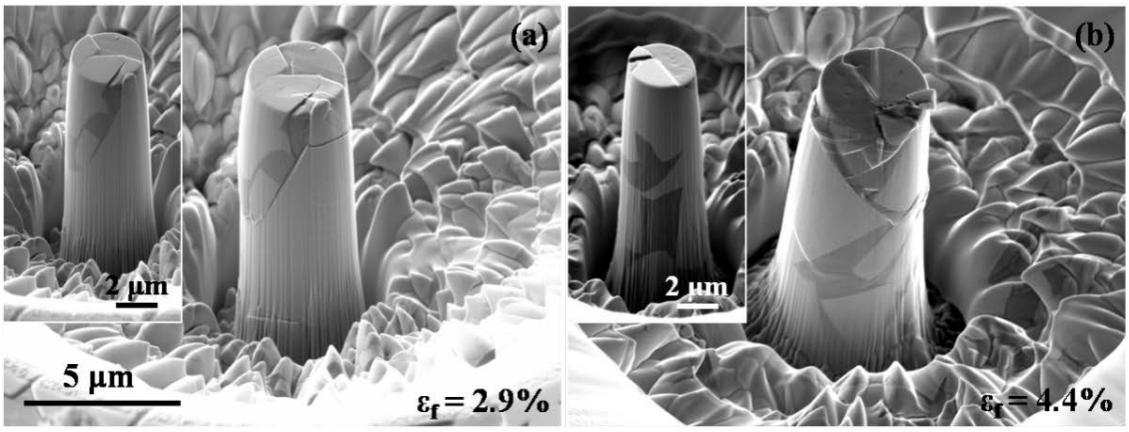

Figure 1. FESEM micrographs of compressed micropillars up to maximum axial deformations of (a) 2.9% and (b) 4.4%. The insets show the appearance of the micropillars before compression. Binder-carbide (within the binder phase) and carbide-carbide interfaces are the weakest points for failure.

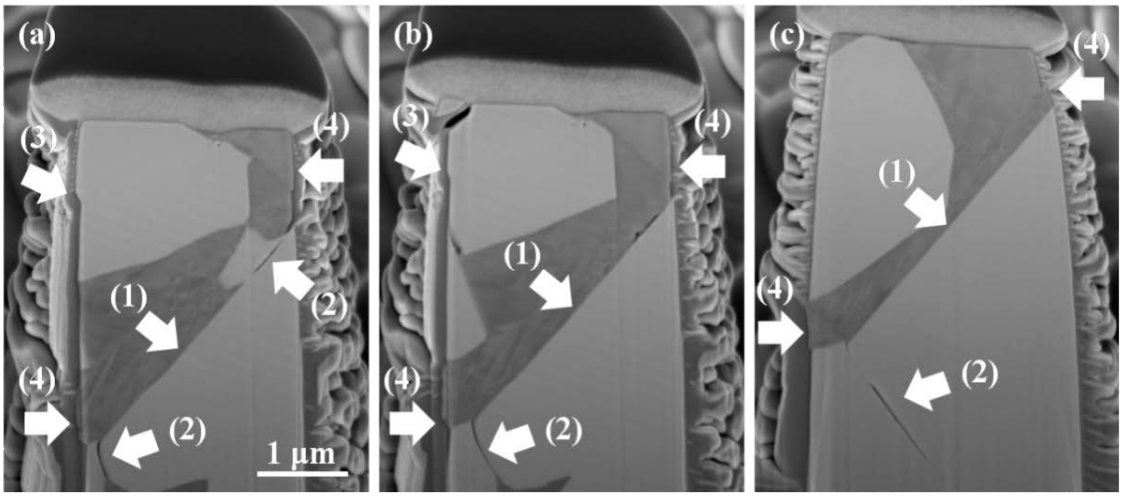

Figure 2. FIB-cross section views corresponding to the micropillar compressed up to a maximal axial strain of 4.4% strain. Different failure mechanisms: (1) glide at the WC/Co interface; (2) cracks in the WC/WC interfaces; (3) activation of a slip system in the WC particle at the top of the pillar; and (4) extensive plastic deformation within the binder, are evidenced and marked with white arrows. All indicated failure events are clearly shown in micrographs (a) and (b). Also, extensive binder plastic deformation is illustrated in micrograph (c).

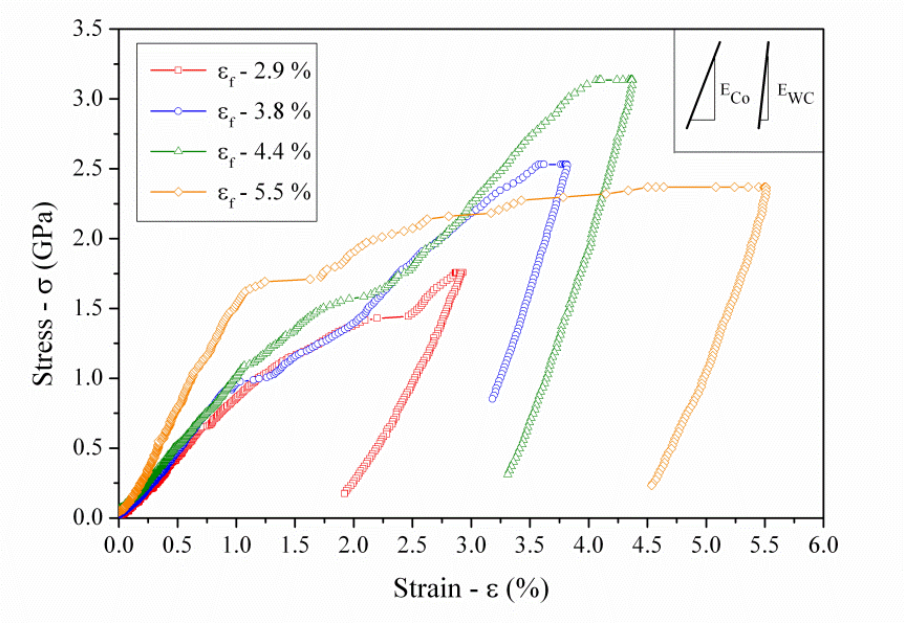

Figure 3. Stress-strain curves resulting from uniaxial compression tests of WC-Co composite micropillars. Several strain bursts are detected at different stress levels. Elastic modulus for tested micropillars, deduced form the unloading stress-strain curves, fits between the Elastic modulus expected for metallic binder and tungsten carbide (provided on the right top corner).

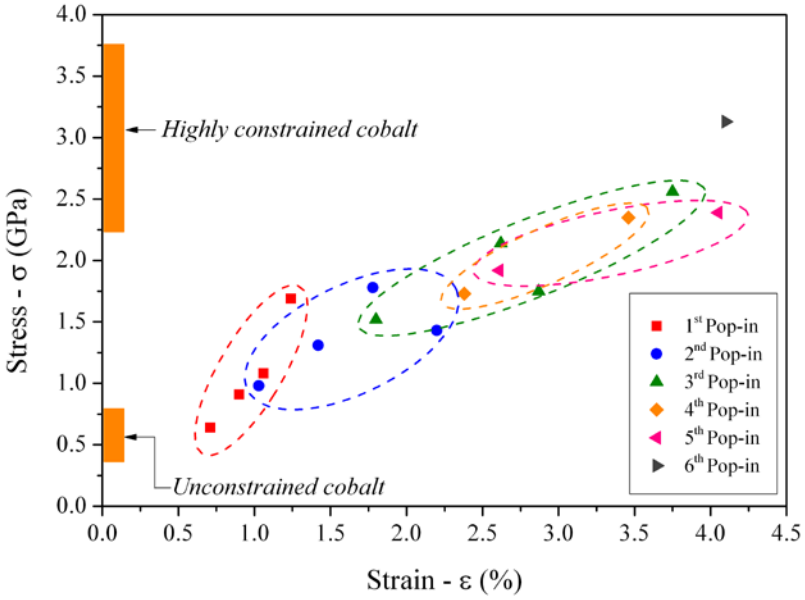

Figure 4. Pop-in events detected in the stress-strain compression curves ranked by their occurrence order. Red bands correspond to the flow stress expected for a completely unconstrained binder (lower level) and a highly constrained metallic phase (upper level).